Royal Society Series on
Advances in Science - Vol.3
英国皇家学会前沿科技丛书——卷3

纳米科技前沿

——电子学、材料和组装

Advances in Nanoengineering

Electronics, Materials and Assembly

英国利兹大学 A.G. 戴维斯
剑桥大学 J.M.T. 汤普森
主编

英文版

机械工业出版社
CHINA MACHINE PRESS

ISBN 978-7-111-36454-2
策划：张金奎/封面设计：张静

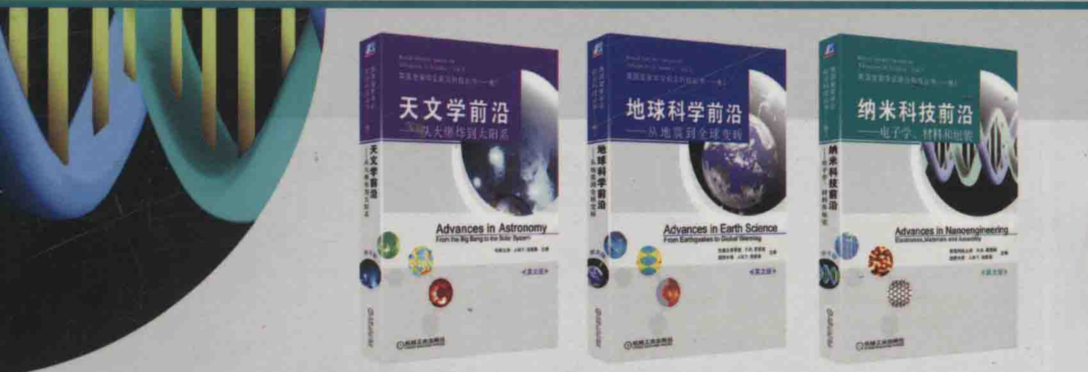

本书主要讲述了当前世界范围内在纳米尺度的现代工程领域中一些激动人心的进展。许多著名科学家和工程师介绍了他们特定科研领域的研究进展，讲述了他们的前沿研究，并提出了他们关于未来的设想。

本书所涵盖的主题有：纳米电子器件、有机导体以及仿生电子学材料的制造与测量；如何将这些结构组装成适当的构型，包括利用生化过程进行组装；有机及无机线、碳纳米管、磁性材料等新材料的研究进展；最后，介绍了这些结构的分析报告及其特征。通过该书，读者可以与作者一起分享他们在现代工程纳米科技前沿工作的兴奋和热情。

对于初入门或正想进入这些厨究领域的青年学者来说，本书不仅可以丰富他们的专业知识、扩展他们的视野，更可以为他们选择适合于自己兴趣的研究方向提供帮助。而对于大学生和那些对这些领域的知识和发展方向有兴趣的一般读者来说，阅读这些书，既可以增进他们的科学知识，也可以助其了解这些领域的发展方向。

地址：北京市百万庄大街22号
电话服务
社服务中心：(010)88361066
销售一部：(010)68326294
销售二部：(010)88379649
读者购书热线：(010)88379203

邮政编码：100037
网络服务
门户网：http://www.cmpbook.com
教材网：http://www.cmpedu.com
封面无防伪标均为盗版

定价：39.00元

ISBN 978-7-111-36454-2
9 787111 364542

CMP BOOKS

英国皇家学会前沿科技丛书——卷3

纳米科技前沿

——电子学、材料和组装

英文版

机械工业出版社
CHINA MACHINE PRESS

英国皇家学会前沿科技丛书——卷

纳米科技前沿

——电子学、材料和组装

主　编　A. G. 戴维斯　（英国利兹大学）

J. M. T. 汤普森　（剑桥大学）

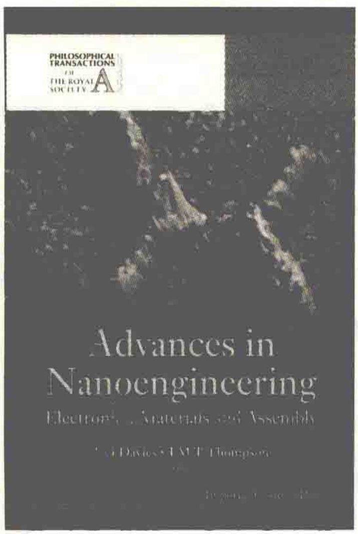

机械工业出版社

A. G. Davies and J. M. T. Thompson: *Advances in Nanoengineering*
Electronics, Materials and Assembly
ISBN 978-1-86094-751-3
Published by Imperial College Press.
Distributed by World Scientific Publishing Co. Pte. Ltd..
English reprint copyright© 2011 by China Machine Press (CMP).

北京市版权局著作权合同登记号：图字 01-2011-4812

图书在版编目(CIP)数据

纳米科技前沿：电子学、材料和组装：英文/（英）戴维斯等主编. —北京：机械工业出版社，2011.11
（英国皇家学会前沿科技丛书；3）
ISBN 978-7-111-36454-2

Ⅰ.①纳…　Ⅱ.①戴…　Ⅲ.①纳米技术—英文　Ⅳ.①TB303

中国版本图书馆 CIP 数据核字（2011）第 233731 号

机械工业出版社(北京市百万庄大街22号　邮政编码100037)
策划编辑：张金奎　责任编辑：张金奎
封面设计：张　静　责任印制：杨　曦
北京圣夫亚美印刷有限公司印刷
2012年1月第1版第1次印刷
148mm×210mm · 10.25印张 · 6插页 · 300千字
标准书号：ISBN 978-7-111-36454-2
定价：39.00元

凡购本书，如有缺页、倒页、脱页，由本社发行部调换

电话服务
社服务中心：(010)88361066
销售一部：(010)68326294
销售二部：(010)88379649
读者购书热线：(010)88379203

网络服务
门户网：http://www.cmpbook.com
教材网：http://www.cmpedu.com
封面无防伪标均为盗版

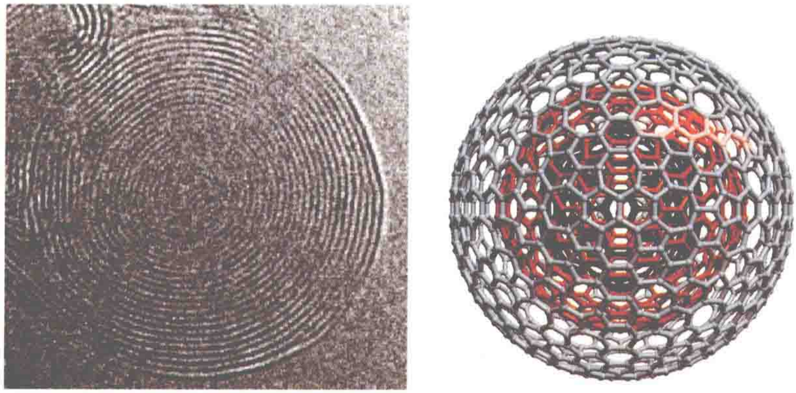

(a) (b)

(a) Spherical carbon onion produced in a TEM at 700°C and (b) model proposed by Terrones and Terrones for spherical carbon onions based on the introduction of additional heptagonal and pentagonal carbon rings (Terrones and Terrones, 1996).

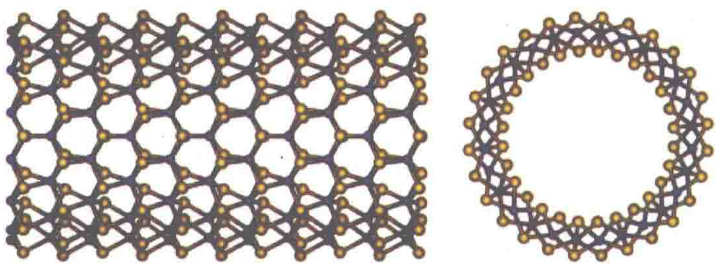

(a)

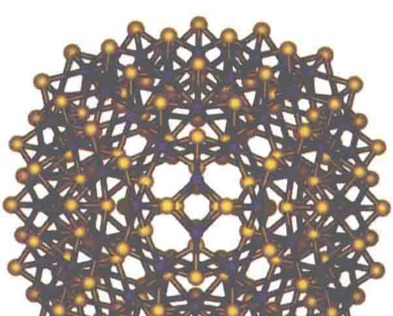

(b)

(a) Molybdenum sulphide zigzag-type nanotube. (b) Molybdenum sulphide octahedral cage.

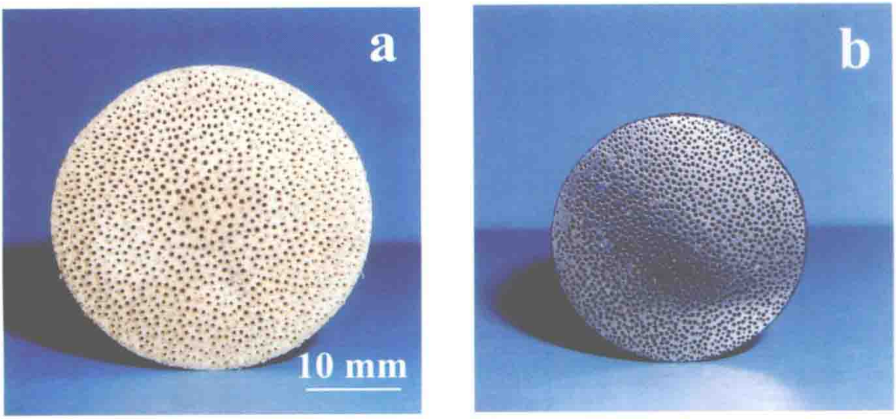

Images of (a) rattan wood and (b) rattan-derived Si–SiC zeolitic bioceramic.

A thin, clear blue film of chitosan/Y124 superconductor precursor.

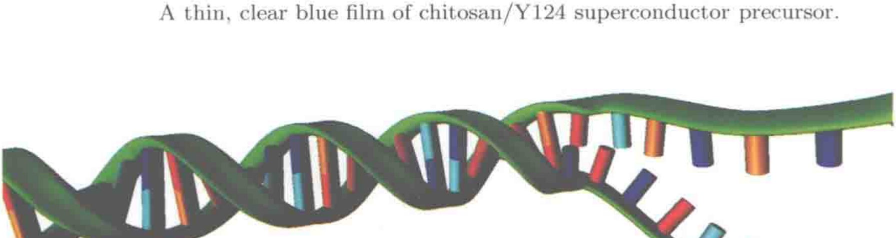

Schematic illustration of double- and single-stranded DNA. The backbone is shown as a green ribbon to which the individual bases are attached. The four different DNA bases are indicated by different colors.

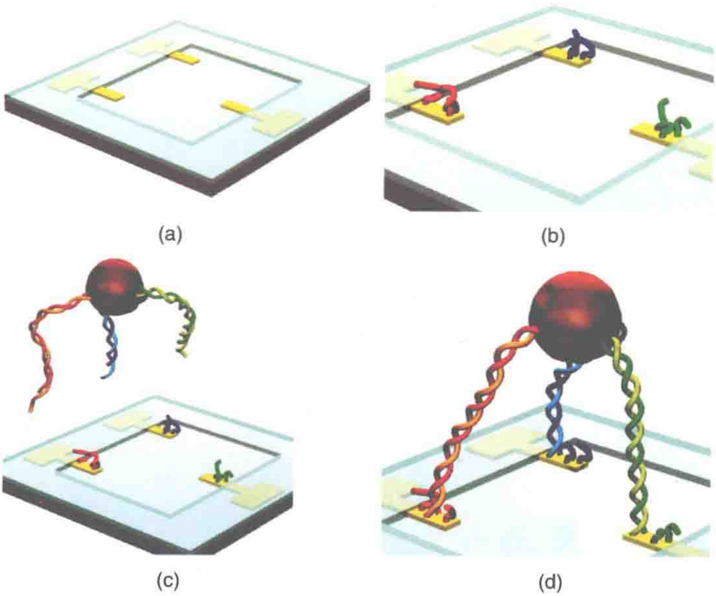

Nanoscale assembly exploiting the molecular self-organization properties of DNA. The three electrodes are functionalized with different single-stranded DNA molecules (b) and the three arms of the molecular complex with the three corresponding complementary DNA oligonucleotides (c). The molecular complex is then assembled onto the device using the self-organizing properties of DNA (d).

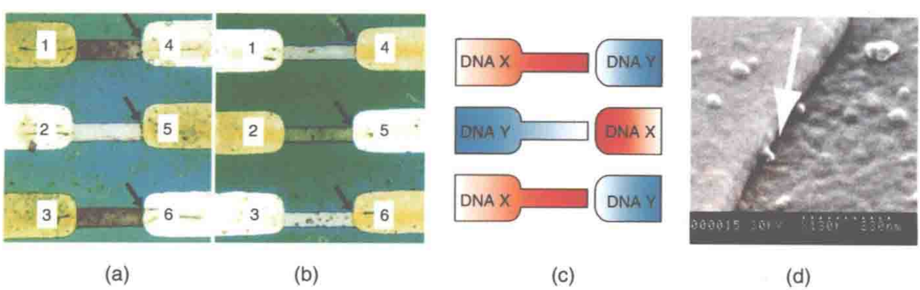

((a), (b)) Electrode arrays with nanoscale gaps separating opposing electrodes (indicated by black arrows). Electrodes 1, 3, and 5 are coated with oligonucleotides **X** and electrodes 2, 4, and 6 with oligonucleotides **Y**. The darker color of the electrodes (a) 1, 3, and 5 indicates the presence of surface-bound oligonucleotides **X**, and (b) of the electrodes 2, 4, and 6 the presence of oligonucleotides **Y**. (c) Schematic of the electrode array. (d) SEM image of the area between two opposing electrodes. The white arrow indicates the gap which appears as a dark line. Reprinted with permission from Ref. 65. Copyright (2003) American Chemical Society.

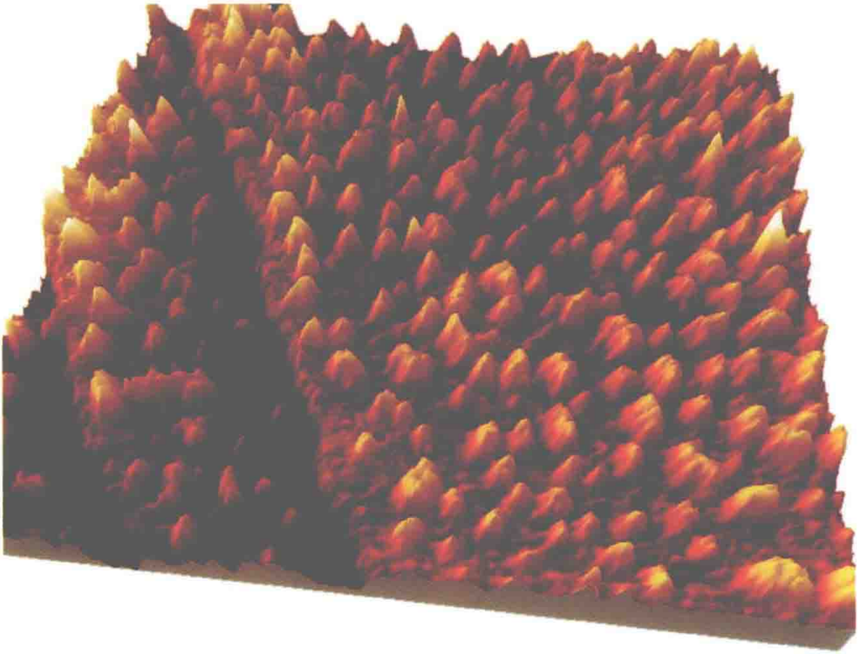

Tunneling image of an array of self-assembled blue copper proteins on an Au[III] electrode surface. The image (approximately 140 nm × 140 nm) was acquired under a water-glycerol mix at room temperature at a tunneling set point of 75 pA (200 mV). These robust molecular layers are generated by using the strong thiol–gold-bonding interactions attainable by adding, genetically, cysteine amino acids to the surface of the metalloprotein. The surface density of these layers can be measured by voltammetric methods to be 1–2 × 10^{13} molecules/cm^2.

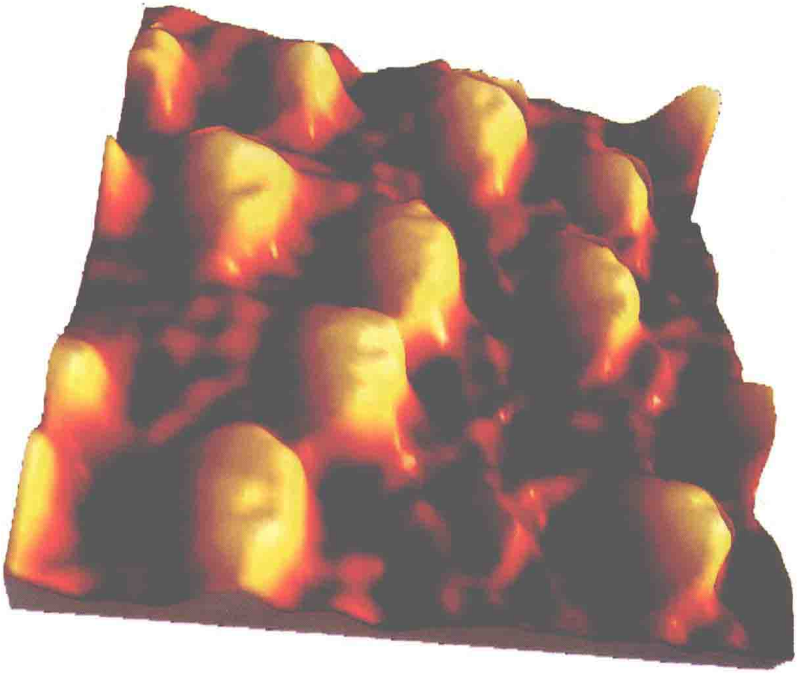

In situ electrochemical STM (10-mM phosphate-buffered saline, pH 7.5; − 0.3 V, 300 pA) of yeast iso-cytochrome *c* molecules adsorbed onto a bare gold electrode surface. Each molecule is approximately 3 nm in diameter and contains one redox-addressable heem group. The role played by the latter in mediating tunneling, under appropriate experimental conditions, can be utilized in "gating" conductance electrochemically (Fig. 3).

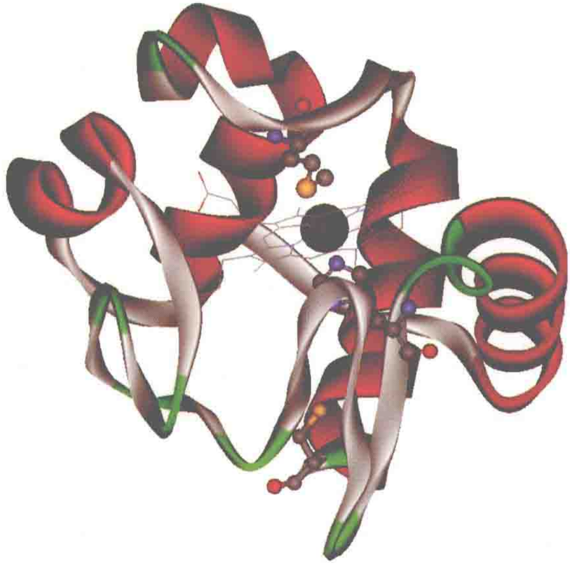

(a) Structure of yeast iso-cytochrome c (pdb IC:1YCC, Ref. 32). The $\sim$3.5-nm diameter, 13-kDa, protein has a heem group which is electrochemically switchable. This particular form of cytochrome c has a solvent-exposed cysteine residue which may usefully be utilized in anchoring the molecule to gold- or sulphur-presenting surfaces. The distance between the thiol and the buried edge of the heem is approximately 1.6 nm.

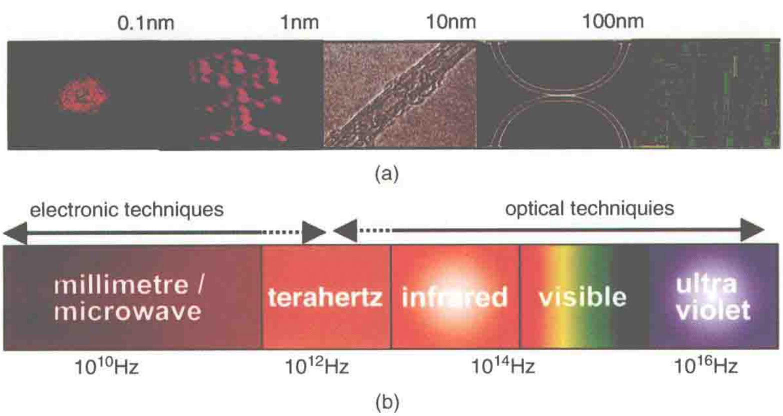

Two limits for modern electronic systems. (a) The size of the system which contains electrons; from left to right in order of increasing size: simulation of electron density around a single atom, carbon monoxide atoms arranged on a platinum surface, a multiwalled carbon nanotube, a semiconductor structure fabricated using electron beam lithography, and a conventional electronic circuit formed using optical lithography. (b) The frequency of operation; the upper frequency range for electronic circuits lies in the low terahertz range, where electronic concepts merge with photonics.

(a)

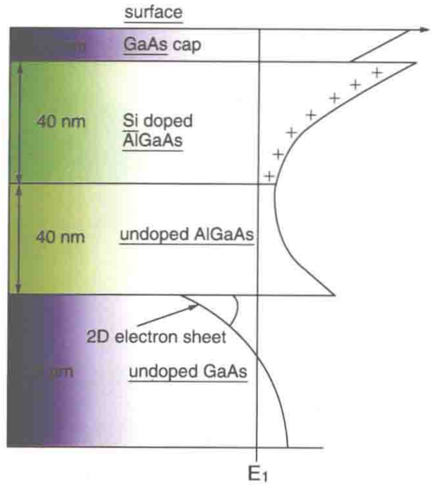

(b)

(a) Photograph of a typical MBE machine, used to grow atomic layers of semiconductor material. (b) Schematic of MBE-grown GaAs/AlGaAs heterostructure wafer structure, and its associated energy profile as a function of depth into the wafer. Electrons from the n-type donar layer migrate to the interface between the undoped AlGaAs and GaAs substrate interface, where confinement causes them to form a 2D electron sheet.

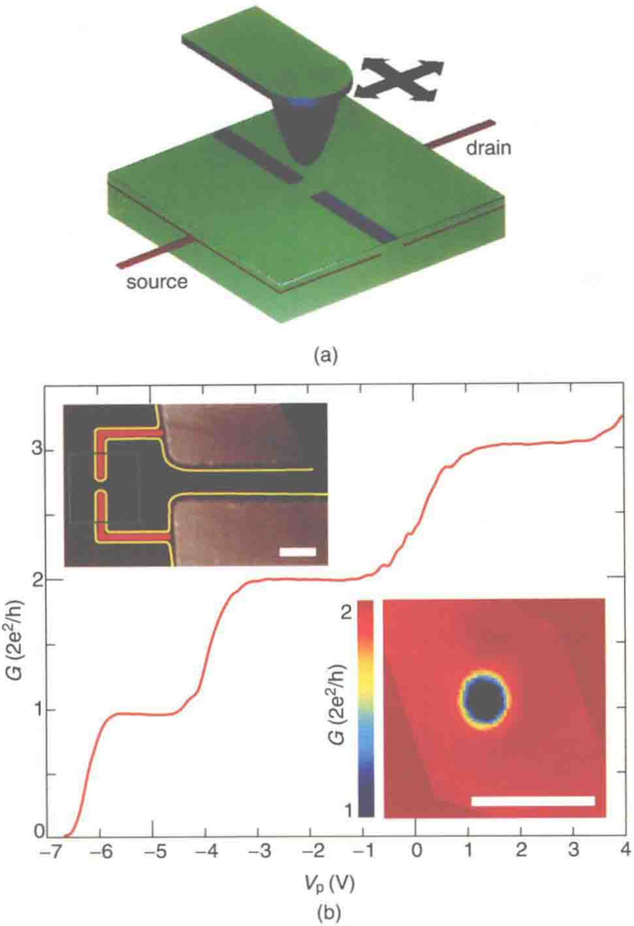

(a) Experimental setup for the study of a quantum wire fabricated by EEL. Negative surface charge is shown in blue. The quantum wire is defined in the subsurface 2DEG, below the gap in the line of surface charge. (b) Plot of device conductance as a function of tip bias and therefore wire width. Plateaus are observed at integer multiples of $2e^2/h$. Upper inset: AFM image of surface electrodes superimposed with surface charge and depletion outlined in yellow. Lower inset: SGM image of the quantum wire made over the region indicated in the upper inset. Scale bar $1\,\mu$m. Parts of this figure were originally published in Ref. 16.

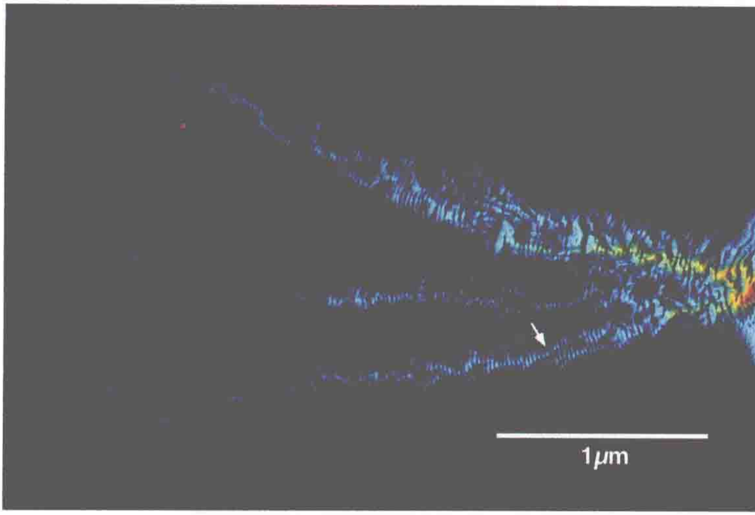

SGM image made over a region to the left of a quantum wire. The arrow indicates a cusp where electron interference is regenerated. Scale bar 1 μm. Figure originally published in Ref. 21.

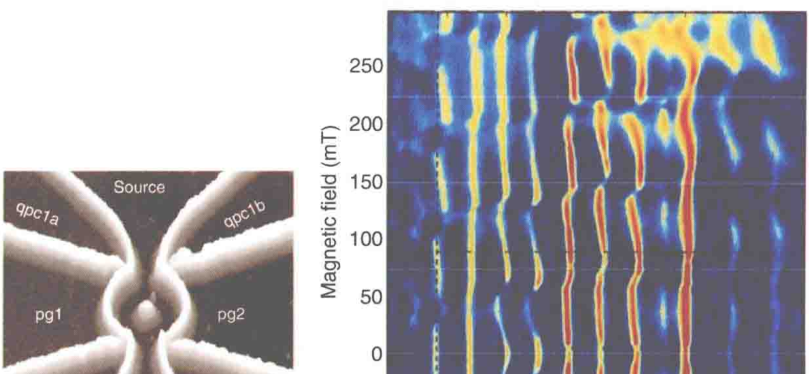

(a) (b)

(a) AFM image of a quantum ring fabricated using LAO. The in-plane gates defined by LAO (qpc1a, qpc1b, qpc2a, qpc2b, pg1, and pg2) are used to tune the size of the quantum wires and the quantum ring. (b) Plot of device conductance as a function of the size of the ring (voltage to pg1 and pg2) and the magnetic field. Coulomb blockade oscillations are seen along the x-axis, and AB-like oscillations along the y-axis. Figure originally published in Ref. 29.

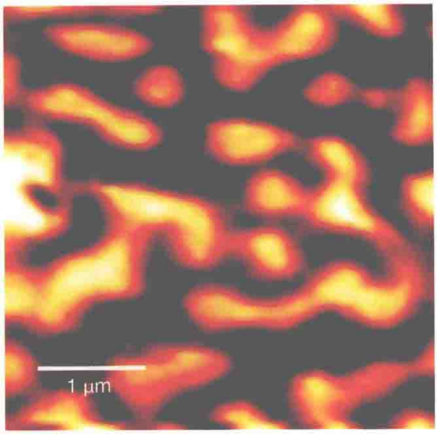

An image of the fluorescence emitted from a blend of two light-emitting polymers, measured using aperture-SNOM. By exciting with carefully chosen wavelengths of light, only one absorbs and then re-emits light.

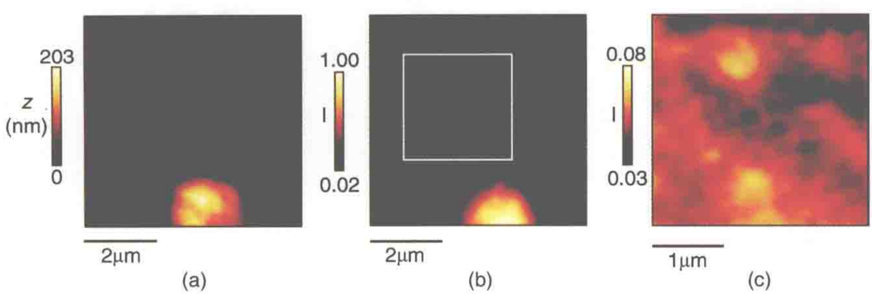

SNOM images of a conjugated polymer blend film containing 10% by weight F8BT and 90% by weight PFB. Intensity (I) is in arbitrary units, and height (z) is in nm. (a) Topographic image. (b) The corresponding fluorescence image for (a). The topographic and fluorescence images were measured simultaneously. (c) An enlarged fluorescence image, taken from the white box shown in (b); the intensity scale is the same as for (b).

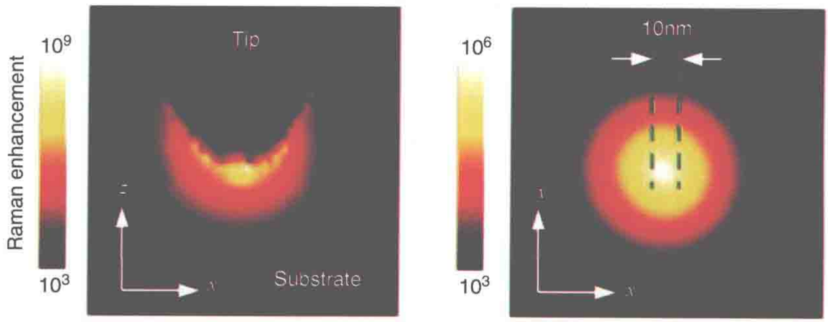

(a) (b)

Calculated enhancement (logarithmic scale) in intensity of Raman scattering in the vicinity of a 20-nm radius metal tip held 4 nm above a glass surface. (a) Cross-section through the tip, along the tip axis. (b) Enhancement in the plane of the sample. The wavelength of illumination is such that a localized mode, strongly confined at the tip apex, is resonantly excited, leading to strong electric field enhancement and hence, Raman scattering.

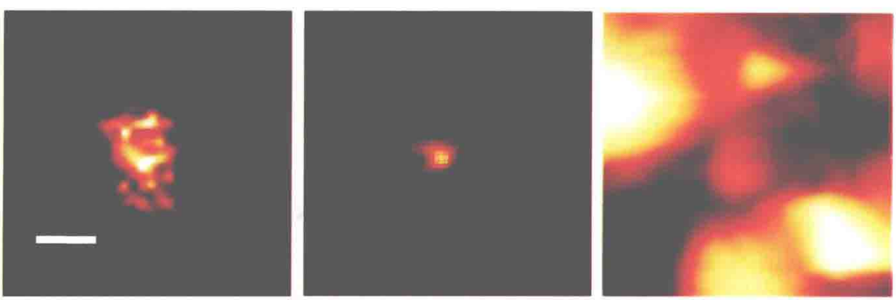

(a) (b) (c)

$1\,\mu m \times 1\,\mu m$ (a) fluorescence confocal (no tip) image (the fluctuations result from intermittent "blinking" of the quantum dot fluorescence), (b) fluorescence apertureless-SNOM image, and (c) topographic image of a small quantum dot cluster. (b) and (c) obtained simultaneously with a sharp gold tip close at the center of the laser focus.

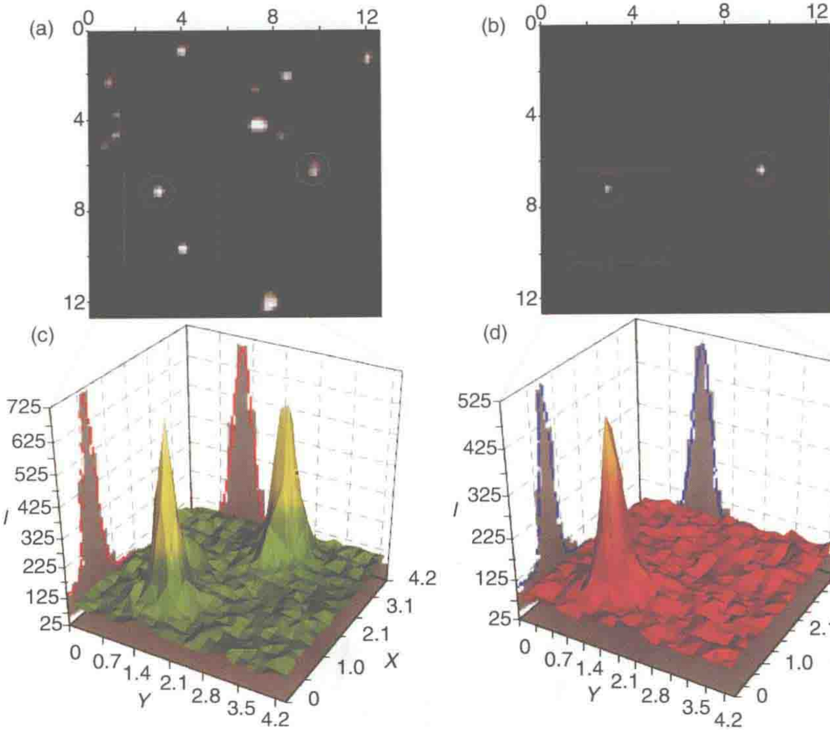

Single molecule localization. Two-color excitation and detection of (a) TMR and (b) Cy5 labeled complimentary 20 mers of DNA. Colocalized molecules are circled on the TMR (green) and Cy5 (red) channels, respectively. The position of each molecule highlighted in the region of interest was measured to an accuracy of (c) $\sigma_{\text{TMR}} = 25\,\text{nm}$ and (d) $\sigma_{\text{Cy5}} = 30\,\text{nm}$ with a minimal detectable separation of $d = (\sigma_{\text{TMR}}{}^2 + \sigma_{\text{Cy5}}{}^2)^{1/2} = 39\,\text{nm}$. The measured peak-to-peak distance of 11 nm, in this case, represents a hybridization event with a false positive of <1 in 2000 at the experimental coverage of ~ 0.1 molecules/μm^2.